Associative detachment of rubidium hydroxide

Jason N. Byrd,[1,2,*] H. Harvey Michels,[1] John A. Montgomery, Jr.,[1] and Robin Côté[1]

[1]*Department of Physics, University of Connecticut, Storrs, Connecticut 06269, USA*
[2]*Quantum Theory Project, University of Florida, Gainesville, Florida 32611, USA*

We performed calculations of the optimized structure, harmonic vibrational frequencies, and dissociation energies of RbOH and its anion, and investigate the interactions between Rb and OH^- leading to possible associative detachment pathways. The electron affinity of RbOH was computed to be 0.2890 eV, with a bond energy of $Rb + OH^-$ half that of $Rb + OH$. To determine other possible charge loss pathways, the $Rb + OH$ and $Rb + OH^-$ dissociation curves were computed using coupled-cluster methods along all possible collisional angles. An adiabatic curve crossing between the neutral and charged molecule was found at the inner wall of the molecular potential curve for linear geometries. Associative detachment rates were estimated using the Langevin ion capture cross section for hydroxide. We find for $v \geqslant 2$ an associative detachment rate of $> 2 \times 10^{-9} \text{ cm}^3\text{s}^{-1}$, while for $v = 0$ and 1 no appreciable rate exists. This strong dependence on vibrational level suggests the ability to control the associative detachment rate directly.

I. INTRODUCTION

Advances in the formation of cold molecules have opened up avenues into many branches of the physical sciences [1,2]. For chemical physics, applications range from precision spectroscopy [3], to the study [4,5] and control [6] of cold chemical reactions. Other areas of physics benefit greatly from the study of cold molecules, such as condensed matter physics [7], and the search for novel quantum gases [8] and phases [9]. Oxides have been of interest recently, such as PbO for electron dipole moment measurements [10], YO [11] for direct cooling, or TiO [12] and the OH radical [13] for trapping. Molecular ions, including oxides, have the added advantage of being more easily trapped and cooled using radio frequency traps and sympathetic cooling [14]. Recent progress on the oxide ion front has seen the co-trapping [15] of cold rubidium and hydroxide.

This successful co-trapping of molecular ions and a cold atomic gas presents the opportunity to investigate chemical reactions involving ionic molecules. A first step towards this is to understand the elastic and inelastic processes involved in the scattering of hydroxide and (cold) rubidium. With low densities characteristic of ultracold gas experiments, we limit ourselves to binary collisions between Rb and OH^-. Possible processes to consider are then elastic collisions that do not change the composition or internal states of the system, quenching reactions that change the internal states of the molecule (such as rotational or vibrational states), rearrangement and combination reactions that exchange atoms (such as $A + BC \rightarrow AB + C$) charge ($A + BC^- \rightarrow A^- + BC$) or combine the atom and molecule together ($A + BC \rightarrow ABC$), and in the case of atom-molecular ion interactions a combination reaction with a loss of an electron (so-called associative detachment illustrated by $A + BC^- \rightarrow ABC + e^-$). In the recent Rb and OH^- co-trapping experiment [15], the observed molecular loss rate was attributed to the associative detachment of hydroxide, a claim strongly motivated by the significant amount of available

energy between the $Rb + OH$ binding energy (~ 3.6 eV) and the electron affinity of OH (~ 1.8). In this work we investigate the interactions of $Rb + OH^-$, and possible associative detachment reaction paths for $Rb + OH^- \rightarrow RbOH + e^-$.

II. ELECTRONIC STRUCTURE CALCULATIONS

Electronic structure calculations were performed on RbH, RbO, OH, RbOH, and associated anions using a combination of perturbation and coupled cluster theory [25]. Second-order Møller-Plesset (MP2) perturbation theory and coupled cluster theory with all singles, doubles, and perturbative triples [CCSD(T)] energy and gradient calculations in this work were carried out using the CFOUR [26] and MOLPRO 2010.1 [27] quantum chemistry packages. Higher order calculations involving CCSDT and CCSDT(Q) (all triples and perturbative quadruples, respectively) were done using the MRCC program of Kállay [28]. For open-shell systems, the spin-restricted variants of these theories were used. Due to the size of rubidium, there are a number of correlation space choices available for consideration. We have adopted the same notation as Sullivan *et al.* [29] where valence-only calculations (H:$1s$; O:$2s2p$; Rb:$5s$) are referred to as relaxed valence (rv). Increasing the correlation space size to involve the first set of subvalence orbitals (H:$1s$; O:$1s2s2p$; Rb:$4s4p5s$) results in the relaxed inner valence (riv), while spaces including yet deeper orbitals (H:$1s$; O:$1s2s2p$; Rb:$3s3p3d4s4p5s$) are called riiv and so forth. Valence-only (rv) calculations involving rubidium and oxygen require extra care, as the usual method of energy sorting orbitals in selecting the frozen core will fail since the energy of the $2s$ orbital of oxygen is below the $4p$ orbital of rubidium. Failing to properly choose the core orbitals for valence calculations will lead to significant errors.

While there are many basis sets available for the first row elements, the basis set selection for rubidium is sparse. This is further complicated by the need for diffuse functions to accurately describe electron affinities [30]. Previous calculations [31,32] involving rubidium using the Karlshruhe def2-nZVPP basis sets [33,34] ($n =$ T,Q zeta quality basis sets with two extra $spdf$ correlation polarization functions)

_____
*byrdja@chem.ufl.edu

TABLE I. Computed bond lengths, harmonic zero-point energies, electron affinities (EA), and atomization energies (AE) for RbOH, its constitutes, and their anions (units are in angstroms, electron volts, and 10^{-3} a.u. as appropriate).

	r(M-H)	r(M-O)	ZPE[a] [16]	EA	AE
OH	0.9698		8.53		162.91
Expt.	0.9696 [17]		8.51 [16]		161.53 [18]
OH$^-$	0.9643		8.55	1.8405	176.51
Expt.	0.9643 [19]		8.51 [19]	1.8277 [20]	175.65 [21]
RbO		2.3548	0.79		102.21
Expt.		2.2541 [22]	0.84 [22]		
RbO$^-$		2.2564	0.65	0.1002	58.90
RbH	2.3919		1.12		61.39
Expt.	2.37 [23]		1.34 [23]		
RbH$^-$	2.5415		1.66	0.3604	47.11
RbOH	0.9551	2.3408	11.72		291.26
Theory	0.959 [24]	2.472 [24]	11.36 [24]		
RbOH$^-$	0.9567	2.4166	11.27	0.2912	247.98

[a]ZPE $\simeq \omega_e/2$.

have shown good experimental agreement for both dissociation energies and bond lengths of the Rb$_2$ diatom. For rubidium these basis sets use the small-core ECP28MWB [35] Stuttgart pseudopotential, which removes the argon core electrons from the calculation while leaving the $4s4p5s$ electrons free for use in further correlation calculations. The addition of even tempered $spdf$ diffuse functions to these basis sets was done to better describe the anion, while the addition of these diffuse functions has also shown to improve molecular properties [36,37] as well. This aug-Def2-nZVPP basis set was used for rubidium in all riv electronic structure calculations in this work. To best describe the OH bond, the optimized aug-cc-pVnZ valence [30] and aug-cc-wCVnZ weighted core-valence [38] correlation basis sets were used for hydrogen and oxygen, respectively.

Molecular structures were optimized using the CCSD(T)/riv level of theory using the quadruple zeta (QZ) quality basis sets.[1] Frequency calculations at the riv CCSD(T) level of theory using the QZ basis sets were performed for each optimized structure to identify whether the structure was a transition state or a local minimum of the potential energy surface. The final ground-state structure of the RbOH$^-$ ion is found to be linear, consistent with the ground-state structure of the neutral molecule [24,39]. Additionally the conformers OHRb$^-$ and ORbH$^-$ were also investigated and found to be transition states. Vibrational harmonic zero-point energy (ZPE) corrections were computed for the final structures at the CCSD(T)/riv level of theory using the QZ basis set. Computed bond lengths and ZPE corrections are listed in Table I.

Correlation calculations involving the riiv electrons of rubidium involve electrons dropped by the MWB pseudopotential. Because of this we perform the riiv correlation calculations all electron using the Roos atomic natural orbital (ANO) basis set [40], which was chosen for its availability

for all atoms present and its noted consistency [41]. Prior to use, the basis set was completely uncontracted so as to be as flexible as possible in subsequent correlation calculations. Scalar relativistic effects were accounted for by adding in the one-electron second-order Douglas-Kroll-Hess [42,43] contribution. For rv and riv calculations, which use the Def2 basis sets for rubidium, the small core MWB family of pseudopotentials has been shown [35] to accurately account for the relativistic contributions to the bond length and dissociation energy.

The complete basis set limit (CBS) of the various contributions to the total energy was estimated using the two-point linear extrapolation formula of Helgaker et al. [44],

$$E_{\text{CBS}}(\text{method}) = \frac{n^3 E_n - (n-1)^3 E_{n-1}}{n^3 - (n-1)^3}. \quad (1)$$

This extrapolation scheme was chosen over other more optimized schemes due to the spread of basis sets and correlation spaces used here. The final interaction energy is computed from the various contributions by the following formula:

$$E_{\text{int}} = E_{\text{CBS}}(\text{CCSD(T)/riv}) + E(\Delta\text{CCSD(T)/riiv}), \quad (2)$$

where $E(\text{CCSD(T)/riv})$ is the total CCSD(T)/riv energy and

$$E(\Delta\text{CCSD(T)/riiv}) = E(\text{CCSD(T)/ANO/riiv})$$
$$- E(\text{CCSD(T)/ANO/riv}) \quad (3)$$

is the riiv contribution. Higher order triples contributions beyond the CCSD(T) level of theory were estimated by performing CCSDT/rv calculations using QZ quality basis sets. Effects of connected quadruple excitations, known [21] to be important for OH$^-$, were estimated using CCSDT(Q)/rv with the triple zeta (TZ) quality basis sets. It was found that the contribution of these higher order terms to the final electron affinity (EA) are small ($<5 \times 10^{-5}$ a.u.) due to cancellation. While the riiv correlation contribution is similarly small for the EA of RbOH at the equilibrium geometry, it becomes more significant for much shorter Rb-O bond lengths (further discussed below). In Table II, the contributions of each of these corrections to the Rb-O bond energy are listed. Molecular bond

---

[1]It should be noted that bond lengths computed using MP2 theory differ only by a few mÅ from CCSD(T) calculations using the same basis set, at a much cheaper computational cost.

TABLE II. Breakdown of the contributions of various levels of theory to the Rb-O bond energy (in 10^{-3} a.u.) for both neutral and charged RbOH.

Method	Space	Rb+OH$^-$	Rb+OH
CCSD(T)/TZ	riv	75.40	129.25
CCSD(T)/QZ	riv	74.63	130.47
CCSD(T)/Extrap.	riv	74.07	131.36
ΔCCSD(T)/ANO	riiv	0.25	0.21
Total energy	–	74.20	131.54

lengths, electron affinities (EA), and atomization energies (AE) (including the harmonic ZPE correction) are reported in Table I. The excellent agreement with available experimental bond lengths, harmonic frequencies, and electron affinities leads us to expect comparable accuracy for the RbOH complex.

III. COMPUTATIONAL RESULTS AND DISCUSSION

The EA and similar geometric structure of rubidium hydroxyl and its anion, along with the large difference in neutral and anion dissociation limits illustrated in Fig. 1, does not suggest immediately a charge loss pathway. In fact, at 300-K no other dissociation channels are energetically accessible. This is clearly illustrated in Fig. 2 where the minimum energy dissociation path of Rb for both RbOH and its anion are computed at the fixed OH bond CCSD(T)/riv/CBS level of theory. It can be seen that the neutral and anion curves do not cross at any point along the incoming path. However it should be noticed that the inner wall of these curves become nearly degenerate at this level of theory. We examine the inner wall more closely, by relaxing the OH bond at each Rb-O distance using MP2 gradients [as noted previously, MP2 bond lengths are very close to CCSD(T) bond lengths], and find that indeed the neutral and anion curves cross at r(Rb-O) ~ 1.81 Å with a barrier height of $V_c(0) \sim 3.0 \times 10^{-2}$ a.u. above the Rb + OH$^-$ dissociation limit, as illustrated in Fig. 3. This crossing energy $V_c(\theta)$ also includes the CCSD(T)/riiv correction which provides $\sim 4 \times 10^{-4}$ a.u. to the final barrier

FIG. 2. Potential energy curve of Rb + OH and its anion computed along the C$_{\infty v}$ axis at the CCSD(T)/CBS level of theory. The OH bond length is held fixed over the entire curve for simplicity. Also shown are the energy asymptotes for various OH$^-$ vibrational levels.

height. This crossing is energetically accessible if the internal rotational and vibrational energy of OH$^-$ is taken into account. In fact, it is well known that producing rotationally and vibrationally cool OH$^-$ is difficult experimentally [19].

The height of $V_c(\theta)$ for geometries other than the linearly minimum energy approach was also investigated. It was found that for small angle approaches, relative to the equilibrium geometry, the crossing remains relatively flat, while for angles greater than 40° the barrier rapidly increases in height until it is completely energetically inaccessible (see Fig. 3).

To evaluate the associative detachment rate coefficient, while accounting for the dependence with the angle of approach, we assume that OH$^-$, in its internal ro-vibrational state (v,J), is rotating sufficiently fast during its encounter with Rb. We then average the angular dependence of $V_c(\theta)$ to obtain an effective angular phase space $\rho_c(v,J,\varepsilon)$ where the
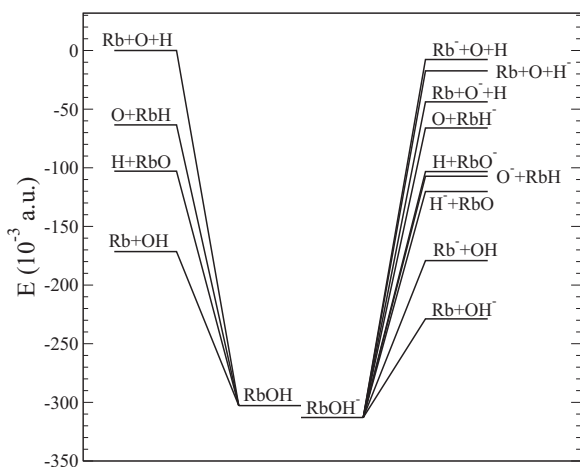

FIG. 1. Dissociation limits of rubidium hydroxyl (left) and its anion (right) up to the atomization limit. Energies are computed at the CCSD(T)/CBS level of theory.
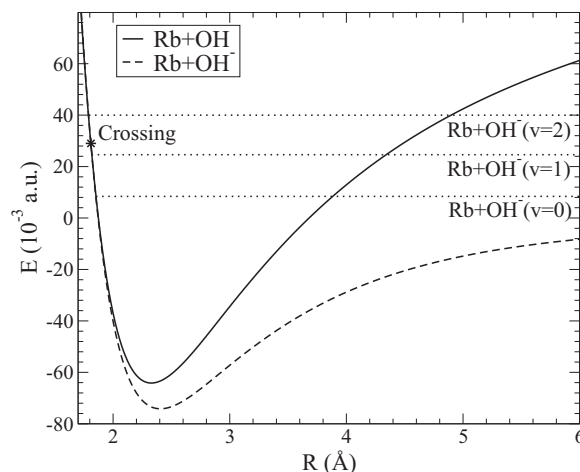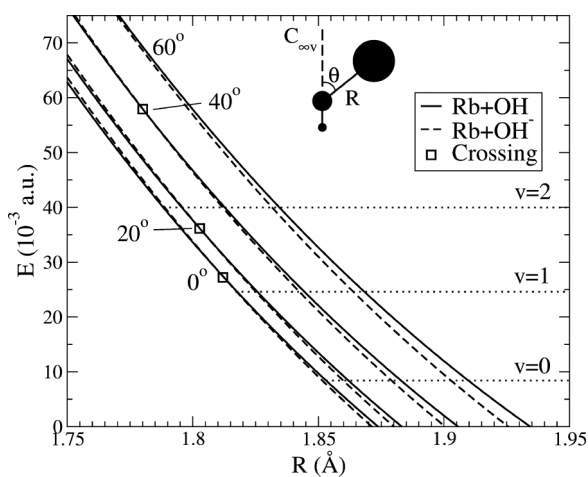

FIG. 3. Inner wall potential energy curve of Rb + OH and its anion computed for various collisional angles at the CCSD(T)/CBS level of theory with the OH bond length relaxed at each point of the curve. The sketch defines the angle θ of the Rb (largest circle) approach to OH$^-$ centered on the oxygen (with O larger than H) from the C$_{\infty v}$ axis.

TABLE III. Representative values of the accessible angular space, Eq. (4), for various vibrational and rotational states for a collisional energy of 300 K.

J	$\rho_c(v,J,300\ \text{K}) \times 100$			
	$v = 0$	$v = 1$	$v = 2$	$v = 3$
0	0.00	0.00	5.38	11.00
5	0.00	0.00	6.56	12.07
10	0.00	3.16	9.53	14.80
15	0.89	8.11	14.00	18.92

curve crossing is accessible for a given collision energy ε,

$$\rho_c(v,J,\varepsilon) = \frac{1}{2} \int_0^\pi d(\cos\theta)\Theta\left[\varepsilon - V_c(\theta) + T(v,J)\right]. \quad (4)$$

Here, the prefactor $\frac{1}{2}$ arises from the azimuthal angle integration, $\Theta(\cdots)$ is a Heaviside step function representing the height of the crossing as a function of the collision angle and for a given collision energy ε, and $T(v,J) = G(v) + F_v(J)$ is the internal rotation-vibration energy of the OH$^-$ fragment in its vth vibrational and Jth rotational state, which we take to follow a Dunham series [45]. The integral over θ involving $V_c(\theta)$ is performed numerically, with representative values presented in Table III for a few J's of $v = 0, \ldots, 3$ at $\varepsilon/k_B = 300$ K (k_B is the Boltzmann constant). We find that $\rho_c(v,J,\varepsilon)$ is negligible for $v = 0$ and $v = 1$ for low J's, and becomes more significant, reaching the range of 10%–20% for $v \geqslant 2$ in this table.

Using this approximation, we estimate the total cross section for associative detachment $\sigma_{\text{tot}}(v,J,\varepsilon)$ by multiplying the Langevin cross section $\sigma_L(\varepsilon)$ for entering the inner region of the Rb + OH$^-$ curve (where the process can take place with assumed unit probability) by the fraction of angular phase space $\rho_c(v,J,\varepsilon)$ allowing the process (i.e., when the curve crossing is accessible),

$$\sigma_{\text{tot}}(v,J,\varepsilon) = \sigma_L(\varepsilon)\rho_c(v,J,\varepsilon). \quad (5)$$
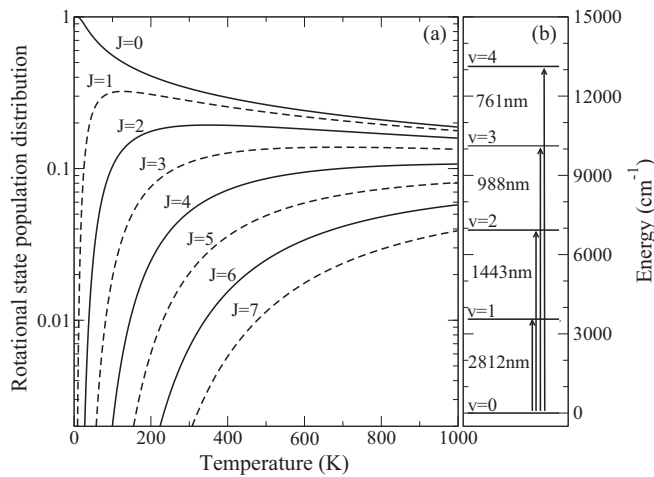

FIG. 4. (a) Rotational state population distribution as a function of temperature for the $v = 0$ state of OH$^-$. Effects on the rotational distribution as a function of vibrational level are quantitative only and vary on the order of 3%. (b) Rotationless vibrational level energies, $T(v,0)$, for OH$^-$ and transition wavelengths from $v = 0$ to various excited vibrational levels.

TABLE IV. Hydroxide anion dipole moments for each vibrational level $\mathcal{D}_v = \langle v|\mathcal{D}(R)|v\rangle$ and transition dipole moments between vibrational levels $\mathcal{R}_{v',v} = \langle v'|\mathcal{D}(R)|v\rangle$. Units are in a.u. and [n] denotes $\times 10^n$.

v	$\mathcal{D}_v$	$\mathcal{R}_{v+1,v}$	$\mathcal{R}_{v+2,v}$	$\mathcal{R}_{v+3,v}$	$\mathcal{R}_{v+4,v}$
0	4.124[−1]	3.676[−2]	−1.161[−3]	4.279[−4]	−1.553[−4]
1	3.822[−1]	−5.301[−2]	2.048[−3]	6.700[−4]	
2	3.478[−1]	−6.919[−2]	−1.604[−3]		
3	3.091[−1]	8.610[−1]			
4	2.660[−1]				

Here, $\sigma_L(\varepsilon)$ depends on the static dipole polarizability α_d of the neutral monomer (with $\alpha_d = 318.6$ for Rb [46]), but not on the inner part of the potential curve [47,48],

$$\sigma_L(\varepsilon) = \pi \sqrt{\frac{2\alpha_d}{\varepsilon}}. \quad (6)$$

A thermal rate constant $k_{\text{ad}}(v,J)$ for the associative detachment for OH$^-$ initially in a specific (v,J) state is obtained by averaging $v\sigma_{\text{tot}}$ over a Maxwell distribution of velocity v characterized by a (translational) temperature T, namely

$$k_{\text{ad}}(v,J) = \sqrt{\frac{2k_BT}{\pi\mu}} \int_0^\infty dx\ x\ e^{-x}\sigma_{\text{tot}}(v,J,xk_BT), \quad (7)$$

where $x = \varepsilon/k_BT$, and μ is the reduced mass of the colliding partners (here Rb and OH$^-$). The distribution of rotational states J is assumed to be thermalized against the collision energy, which gives the vibrational state rate constant,

$$k_{\text{ad}}(v) = \frac{1}{Q_{\text{rot}}} \sum_J^{J_{\text{max}}} k_{\text{ad}}(v,J) \exp\left(-\frac{F_v(J)}{k_BT}\right), \quad (8)$$

TABLE V. Spontaneous emission rotational rate coefficients, Eq. (10), for OH$^-$ in various starting rotational and vibrational levels. Units are in inverse seconds and [n] represents $\times 10^n$.

| J'	$A_{v'\to v}(J')$ (s^{-1})					
	$1 \to 0$	$2 \to 0$	$2 \to 1$	$3 \to 0$	$3 \to 1$	$3 \to 2$
0	6.87[1]	5.16[1]	1.22[2]	2.19[1]	1.36[0]	1.75[2]
1	2.36[2]	1.78[0]	4.18[2]	7.54[1]	4.68[0]	6.00[2]
2	4.34[2]	3.26[0]	7.68[2]	1.38[0]	8.58[0]	1.10[3]
3	6.31[2]	4.72[0]	1.12[3]	2.00[0]	1.24[1]	1.61[3]
4	8.30[2]	6.20[0]	1.47[3]	2.63[0]	1.64[1]	2.12[3]
5	1.03[3]	7.70[0]	1.83[3]	3.27[0]	2.03[1]	2.64[3]
6	1.24[3]	9.23[0]	2.21[3]	3.91[0]	2.44[1]	3.19[3]
7	1.46[3]	1.08[1]	2.60[3]	4.58[0]	2.86[1]	3.76[3]
8	1.69[3]	1.24[1]	3.01[3]	5.26[0]	3.29[1]	4.36[3]
9	1.92[3]	1.41[1]	3.43[3]	5.97[0]	3.74[1]	4.98[3]
10	2.17[3]	1.59[1]	3.88[3]	6.71[0]	4.20[1]	5.65[3]
11	2.43[3]	1.77[1]	4.36[3]	7.47[0]	4.69[1]	6.36[3]
12	2.70[3]	1.96[1]	4.86[3]	8.27[0]	5.20[1]	7.11[3]
13	3.00[3]	2.16[1]	5.40[3]	9.10[0]	5.74[1]	7.91[3]
14	3.30[3]	2.36[1]	5.97[3]	9.97[0]	6.30[1]	8.77[3]
15	3.63[3]	2.58[1]	6.57[3]	1.09[1]	6.89[1]	9.69[3]
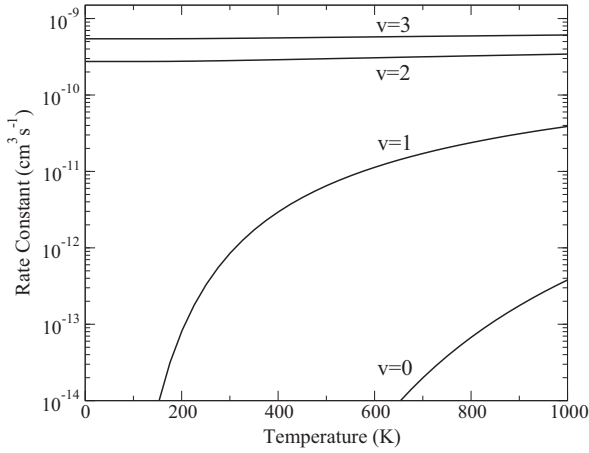
FIG. 5. Ion capture rate coefficient as a function of the collisional temperature of the OH^- complex for the first four vibrational levels.

with the rotational partition function given by

$$Q_{\text{rot}} = \sum_J^{J_{\max}} \exp\left(-\frac{F_v(J)}{k_B T}\right). \quad (9)$$

Here $J_{\max}$ is the maximum rotational state taken in the series. To evaluate Eq. (8) we use the spectroscopic constants of Rosenbaum *et al.* [19] in $T(v,J)^2$ and choose $J_{\max}$ such that the thermodynamic contribution of that rotational state is negligible [see Fig. 4(a)]. A value of $J_{\max} = 15$ was found to be more than adequate to converge the sums in Eqs. (8) and (9) even for very high temperatures. The rate constant (8) was evaluated numerically for the first three vibrational levels of OH^- as a function of the collisional temperature, the results of which are plotted in Fig. 5. The rate constant for $v = 0$ and $v = 1$ is found to be much lower than a recent experimental value [15], but becomes comparable for $v = 2$, as expected considering the energetics of the collision. It should be noted that for $v = 2$ and higher, the incoming collisional energy is above the curve crossing threshold, and so the rate coefficient is a nearly constant as expected.

As these collisions involve rotationally and vibrationally excited states of a polar molecule, it is important to characterize the lifetime of these states in the absence of collisions. To do this we have computed the OH^- potential energy curve near the equilibrium geometry at the $E_{\text{CBS}}(\text{CCSD(T)/riv})$ level

___

[2]$B_e = 19.120\,87$ cm^{-1}, $\alpha_e = 0.771\,67$ cm^{-1}, $\omega_e = 3738.44$ cm^{-1}, and $\omega_e x_e = 91.42$ cm^{-1} [19].

TABLE VI. Temperature-dependent vibrational state lifetimes averaged over initial rotational states. Units are in kelvin and miliseconds.

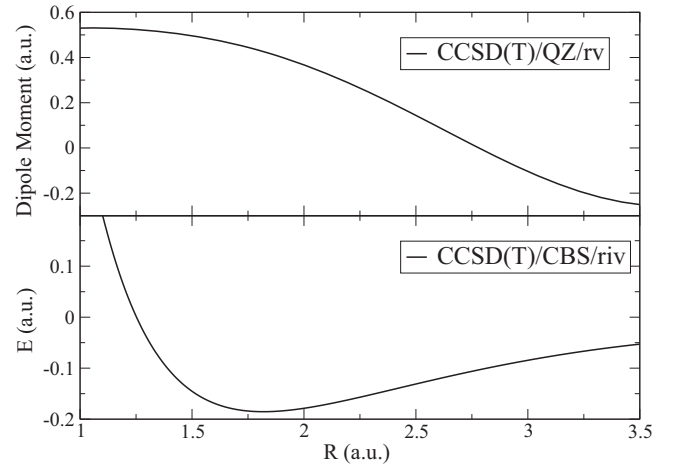| Temperature (K)	$v' = 1$	$v' = 2$	$v' = 3$
10	14.5	8.17	5.67
100	9.94	5.60	3.88
300	6.98	3.93	2.72
600	5.44	3.06	2.12

FIG. 6. Computed static dipole moment (top) and potential energy curve (bottom) for OH^- near equilibrium.

of theory as well as the static dipole moment $\mathcal{D}(R)$ along this curve at the CCSD(T)/rv level of theory using the aug-cc-pVQZ basis set (see Fig. 6). We find that the resulting vibrational dipole and transition dipole moment values to be in good agreement with the original work of Werner *et al.* [49] and have tabulated the results in Table IV. The spontaneous emission rate for a given initial rotational and vibrational state J', v' radiating to all possible lower energy rotational states is (in atomic units) [50] given by

$$A_{v' \to v}(J') = \sum_J \frac{4}{3}\alpha^3(T(v',J') - T(v,J))^3$$
$$\times \langle v'; J'M'\Omega'|\mathcal{D}(R)|JM\Omega; v\rangle, \quad (10)$$

where $|v\rangle$ is the vibrational wave function for the vth level and $|JM\Omega\rangle$ is the rigid-rotor wave function [51]. We have tabulated our results for $A_{J',v' \to v}$ in Table V for all J' up to $J_{\max}$, for the various vibrational transitions for $v = 0$ through $v = 3$ [see Fig. 4(b)]. Given an initial vibrational state, the temperature-dependent lifetime averaged over the rotational level is

$$\tau_{v'} = \frac{1}{Q_{\text{rot}}} \sum_v \sum_J^{J_{\max}} \frac{\exp(-F_v(J)/k_B T)}{A_{v' \to v}(J')}. \quad (11)$$

In Table VI the lifetimes for the first three excited vibrational levels are listed at several representative temperatures.

IV. CONCLUSIONS

We have computed CCSD(T) *ab initio* potential energy curves for the Rb + OH and Rb + OH$^-$ systems, and found a neutral-ion curve crossing along the inner wall of the potential energy curve for collinear geometries of RbOH. Further investigation of the potential energy surface shows that this crossing is highly dependent on the collisional angle and is accessible at low scattering energies only for angles near the collinear geometry. Furthermore, this crossing lies above the OH^- ($v = 0$) collisional threshold, and so is expected to have a negligible contribution to the loss of OH^- and the long-term co-trapping of rubidium and hydroxide. From the thermal

rotational state distribution results shown in Fig. 4(a) a large fraction of the trapped OH^- molecules will be rotationally excited in $J \geqslant 3$. Quenching collisions involving OH^- that lead to $J \geqslant 3 \to J' = 0$ transitions release over 300 K in kinetic energy [52], which is sufficient to kick hotter ions out of the trap making this a significant molecular loss process for experiments with small trap depths. This quenching process can be mitigated by longer exposure to the initial neon buffer gas (as used by Deiglmayr *et al.* [15]) or by a different choice in buffer gas such as helium (which provides a more favorable reduced mass ratio).

Using the Langevin capture cross section, we evaluated the associative detachment rate for the first few vibrationally excited states of hydroxide colliding with rubidium and found an appreciable rate coefficient $> 2 \times 10^{-9}$ cm^{3}s^{-1} for hydroxide vibrational levels $v \geqslant 2$. The optical transition to vibrational states greater than $v = 2$ lies in the near infrared to visible spectrum [see Fig. 4(b)], which is experimentally accessible with standard lasers. Because of the sharp difference in reaction rates between $v = 0, 1$ and $v \geqslant 2$ (several orders of magnitude as shown in Fig. 5), it is possible to directly probe and control the associative detachment reaction $OH^- + Rb \to RbOH + e^-$. As this process involves vibrationally excited states of OH^- it is necessary to estimate the lifetimes of these states. We have computed the lifetimes of the first three vibrational states as a function of temperature in Table VI and found them to be on the order of 5 ms. These results suggest a promising avenue for experimentally directly investigating and controlling a chemical reaction involving both bond formation and electron detachment.

[1] L. Carr, D. DeMille, R. Krems, and J. Ye, New J. Phys. **11**, 055049 (2009).

[2] O. Dulieu, R. Krems, M. Weidemüller, and S. Willitsch, Phys. Chem. Chem. Phys. **13**, 18703 (2011).

[3] D. DeMille, S. Sainis, J. Sage, T. Bergeman, S. Kotochigova, and E. Tiesinga, Phys. Rev. Lett. **100**, 043202 (2008).

[4] M. de Miranda, A. Chotia, B. Neyenhuis, D. Wang, G. Quéméner, S. Ospelkaus, J. Bohn, J. Ye, and D. Jin, Nature Physics **7**, 502 (2011).

[5] B. Sawyer, B. Stuhl, M. Yeo, T. Tscherbul, M. Hummon, Y. Xia, D. P. J. Klos, J. Doyle, and J. Ye, Phys. Chem. Chem. Phys. **13**, 19059 (2011).

[6] G. Quéméner and P. Julienne, Chem. Rev. **112**, 4949 (2012).

[7] A. Micheli, G. K. Brennen, and P. Zoller, Nat. Phys. **2**, 341 (2006).

[8] L. Santos, G. V. Shlyapnikov, P. Zoller, and M. Lewenstein, Phys. Rev. Lett. **85**, 1791 (2000).

[9] A. Recati, P. O. Fedichev, W. Zwerger, and P. Zoller, Phys. Rev. Lett. **90**, 020401 (2003).

[10] D. DeMille, F. Bay, S. Bickman, D. Kawall, D. Krause, S. E. Maxwell, and L. R. Hunter, Phys. Rev. A **61**, 052507 (2000).

[11] M. T. Hummon, M. Yeo, B. K. Stuhl, A. L. Collopy, Y. Xia, and J. Ye, Phys. Rev. Lett. **110**, 143001 (2013).

[12] B. K. Stuhl, B. C. Sawyer, D. Wang, and J. Ye, Phys. Rev. Lett. **101**, 243002 (2008).

[13] B. Stuhl, M. Hummon, M. Yeo, G. Quéméner, J. Bohn, and J. Ye, Nature (London) **492**, 396 (2012).

[14] S. Schiller and B. Roth, in *Cold Molecules, Theory, Experiment and Applications*, edited by R. V. Krems, W. C. Stwalley, and B. Friedrich (CRC Press, Boca Raton, 2009), Chap. 18.

[15] J. Deiglmayr, A. Göritz, T. Best, M. Weidemüller, and R. Wester, Phys. Rev. A **86**, 043438 (2012).

[16] M. Abrams, S. Davis, M. Rao, R. Engleman, Jr., and J. Brault, Astrophys. J. Suppl. Ser. **93**, 351 (1994).

[17] T. Amano, J. Mol. Spectrosc. **103**, 436 (1984).

[18] K. P. Huber and G. Herzberg, *Constants of Diatomic Molecules* (Van Nostrand Reinhold, New York, 1979).

[19] N. Rosenbaum, J. Owrutsky, L. Tack, and R. Saykally, J. Chem. Phys. **84**, 5308 (1986).

[20] J. R. Smith, J. B. Kim, and W. C. Lineberger, Phys. Rev. A **55**, 2036 (1997).

[21] J. Martin, Spectrochimica Acta Part A **57**, 875 (2001).

[22] C. Yamada and E. Hirota, J. Chem. Phys. **110**, 2853 (1999).

[23] H. Katôx, Y. Toyasaka, and T. Suzuki, Bull. Chem. Soc. Jpn. **58**, 562 (1985).

[24] E. Lee and T. Wright, J. Phys. Chem. A **107**, 5233 (2003).

[25] K. Raghavachari, G. W. Trucks, J. A. Pople, and M. Head-Gordon, Chem. Phys. Lett. **157**, 479 (1989).

[26] J. F. Stanton, J. Gauss, M. E. Harding, P. G. Szalay, A. A. Auer, R. J. Bartlett, U. Benedikt, C. Berger, D. E. Bernholdt, Y. J. Bomble, O. Christiansen, M. Heckert, O. Heun, C. Huber, T.-C. Jagau, D. Jonsson, J. Juslius, K. Klein, W. J. Lauderdale, D. A. Matthews, T. Metzroth, D. P. O'Neill, D. R. Price, E. Prochnow, K. Ruud, F. Schiffmann, S. Stopkowicz, J. Vzquez, F. Wang, and J. D. Watts, http://www.cfour.de.

[27] H.-J. Werner, P. J. Knowles, F. R. Manby, M. Schütz *et al.*, computer code MOLPRO, Version 2010.1, a package of *ab initio* programs, 2010, http://www.molpro.net.

[28] M. Kállay and P. Surján, J. Chem. Phys. **115**, 2945 (2001).

[29] M. Sullivan, M. Iron, P. Redfern, J. Martin, L. Curtiss, and L. Radom, J. Phys. Chem. A **107**, 5617 (2003).

[30] R. Kendall, T. Dunning, Jr., and R. Harrison, J. Chem. Phys. **96**, 6796 (1992).

[31] J. N. Byrd, J. A. Montgomery, Jr., and R. Côté, Phys. Rev. A **82**, 010502(R) (2010).

[32] J. N. Byrd, H. H. Michels, J. A. Montgomery, Jr., R. Côté, and W. C. Stwalley, J. Chem. Phys. **136**, 014306 (2012).

[33] F. Weigend, F. Furche, and R. Ahlrichs, J. Chem. Phys. **119**, 12753 (2003).

[34] F. Weigend and R. Ahlrichs, Phys. Chem. Chem. Phys. **7**, 3297 (2005).

[35] T. Leininger, A. Nicklass, W. Küchle, H. Stoll, M. Dolg, and A. Bergner, Chem. Phys. Lett. **255**, 274 (1996).

[36] D. Rappoport and F. Furche, J. Chem. Phys. **133**, 134105 (2010).

[37] J. N. Byrd, R. Côté, and J. A. Montgomery, Jr., J. Chem. Phys. **135**, 244307 (2011).

[38] K. Peterson and T. Dunning, Jr., J. Chem. Phys. **117**, 10548 (2002).

[39] M. Lara, J. L. Bohn, D. E. Potter, P. Soldán, and J. M. Hutson, Phys. Rev. A **75**, 012704 (2007).

[40] B. Roos, V. Veryazov, and P.-O. Widmark, Theor. Chem. Acc. **111**, 345 (2004).

[41] J. Hill, Int. J. Quantum Chem. **113**, 21 (2013).

[42] M. Douglas and N. M. Kroll, Ann. Phys. (NY) **82**, 89 (1974).

[43] A. Wolf, M. Reiher, and B. A. Hess, J. Chem. Phys. **117**, 9215 (2002).

[44] T. Helgaker, W. Klopper, H. Koch, and J. Noga, J. Chem. Phys. **106**, 9639 (1997).

[45] J. Dunham, Phys. Rev. **41**, 713 (1932).

[46] A. Derevianko, W. R. Johnson, M. S. Safronova, and J. F. Babb, Phys. Rev. Lett. **82**, 3589 (1999).

[47] R. D. Levine and R. B. Bernstein, *Molecular Reaction Dynamics and Chemical Reactivity* (Oxford University Press, New York, 1987).

[48] R. Côté and A. Dalgarno, Phys. Rev. A **62**, 012709 (2000).

[49] H.-J. Werner, P. Rosmus, and E.-A. Reinsch, J. Chem. Phys. **79**, 905 (1983).

[50] The conversion from atomic units to inverse seconds used in this work is $1/(2.419 \times 10^{-17}$ s$)$.

[51] J. Brown and A. Carrington, *Rotational Spectroscopy of Diatomic Molecules* (Cambridge University Press, Cambridge, 2003).

[52] $F_0(3) - F_0(0) = 337$ K to be precise.